Desalination and Water Treatment
www.deswater.com

37 (2012) 114–121
January

doi: 10/5004/dwt.2012.2526

Taylor & Francis
Taylor & Francis Group

Development of stabilized zero valent iron nanoparticles[1]

Lauren F. Greenlee*, Stephanie A. Hooker

National Institute of Standards and Technology, Materials Reliability Division, Boulder, CO USA
Tel. +1-303-497-4234; Fax: +1-303-497-5030; email: lauren.greenlee@nist.gov

Received 10 December 2010; Accepted 20 June 2011

ABSTRACT

Many organic micropollutants have recently been identified in natural water sources and treated drinking water. Often, these compounds are not successfully degraded or removed by current water treatment processes. There is an increasing interest in developing new water treatment technologies based on catalytic nanoparticles to take advantage of enhanced particle reactivity at the nanoscale. Our current research focuses on the development and characterization of zero valent iron (ZVI) nanoparticles to improve nanoparticle design and enhance particle reactivity. The focus of this study was to evaluate two different iron salts as starting materials and to evaluate three different carboxymethyl cellulose stabilizers. The stabilizers were evaluated for their ability to stabilize ZVI nanoparticles during synthesis and to produce dispersed nanoparticles with narrow size distributions. Nanoparticles with a modal particle diameter of less than 50 nm were obtained. Particles were characterized using electron microscopy, dynamic light scattering, thermogravimetric analysis, and zeta potential.

Keywords: Carboxymethyl cellulose; Nanoparticle characterization; Organic contaminant; Zero valent iron; Stabilizer; Nanoparticle synthesis

1. Introduction

As an increasing number of micropollutants including pharmaceuticals, personal care products, industrial chemicals, and disinfection by-products are identified in drinking water sources, water treatment technologies must be developed to target and remove these compounds. A promising area of research within membrane filtration is the development of new membrane materials based on composite polymer-particle systems. Nanosized particles are of particular interest due to the enhancement in surface reactivity that occurs as the particle size decreases. Studies have shown that the large increase in the surface-area-to-volume ratio of nanoparticles causes changes to particle properties such as surface energy, magnetism, and reactivity [1,2]. A review of size-dependent nanoparticle properties revealed that there may be a threshold (30 nm to 40 nm particle diameter) above which nanosized particles behave similarly to micrometer-sized particles, rather than display unique behaviors [3].

Iron-based catalytic nanoparticles have been shown to catalyze oxidative or reductive degradation of organic water contaminants [4–7]. The form of iron typically used is zero valent iron (ZVI). As a reductive system, ZVI nanoparticles have been used to successfully degrade compounds such as trichloroethylene by replacing all three chlorine atoms with hydrogen [8]. The ultimate goal of developing these nanoparticle systems is to incorporate the nanoparticles into membrane matrices to create active membrane systems that both degrade and filter out water contaminants [9]. However, some of the challenges in developing nanoparticles for the treatment of water contaminants are to control the particle size distribution, limit particle aggregation, and increase particle reactivity. This requires stabilization of the particle surface during synthesis.

*Corresponding author.

[1]Contribution of NIST, an agency of the US government; not subject to copyright in the United States.

The use of different starting materials (stabilizers and iron salts), along with thorough characterization of stabilized nanoparticles, are necessary to understand how the stabilizers affect particle aggregation and size, as well as to guide the design of nanoparticle treatment systems. Several iron salts have been used to make ZVI nanoparticles, and there appear to be differences in iron-stabilizer complexation, particle stability, and crystallinity [10,11]. A variety of organic compounds have been tested as stabilizers, including humic acid, surfactants, and glucose-based polymers such as starch and carboxymethyl cellulose (CMC) [12–16]. In particular, CMC compounds have been shown to impart improved particle stability due to the presence of carboxyl functional groups in addition to hydroxyl groups already present in cellulose. Degradation studies performed on unstabilized and CMC-stabilized ZVI nanoparticles strongly suggest that CMC stabilization increases nanoparticle reactivity and therefore contaminant degradation [16].

In this study, the objective was to evaluate ferrous sulfate ($FeSO_4$*$7H_2O$) and ferric chloride ($FeCl_3$) as sources of iron for particle synthesis, as well as evaluate three CMC compounds with varying degrees of substitution of the carboxyl functional group. Particle size, composition, and morphology were characterized by electron microscopy, dynamic light scattering, thermogravimetric analysis, and zeta potential.

2. Materials and methods[2]

2.1. Chemicals

All chemicals used were American Chemical Society (ACS) reagent grade. Ferrous sulfate ($FeSO_4$*$7H_2O$), ferric chloride (anhydrous $FeCl_3$), sodium borohydride ($NaBH_4$), and carboxymethyl cellulose (CMC) were purchased and used as received. Three CMC compounds with a molecular weight of 250,000 g/mole were tested; the degrees of substitution were 0.7, 0.9, and 1.2. All solutions were made with purified and deionized water.

2.2. Nanoparticle preparation

The nanoparticle synthesis method was based on the work of He and Zhao [13]. All synthesis reactions were performed in a glass round bottom flask, and mixing was achieved with an orbital shaker at 100 rpm. For unstabilized nanoparticles, a solution of 1 g/l iron (5.0 g/l $FeSO_4$*$7H_2O$ or 2.9 g/l $FeCl_3$) was flushed with argon for at least 10 min. Particle synthesis was initiated by adding $NaBH_4$ dropwise while mixing by hand. Due to the competing reaction between BH_4^- and water, $NaBH_4$ was added in slight (10%) excess of the stoichiometric requirement (BH_4:Fe molar ratio of 2:1 for $FeSO_4$*$7H_2O$ or 3:1 for $FeCl_3$) for complete reaction of the iron. After $NaBH_4$ addition, the solution was mixed under vacuum until the reaction finished (when the evolution of $H_{2(g)}$ ceased). The particles produced by the reaction are assumed to be primarily zero valent iron, based on previous work [10,12,17]. Excess dissolved salt was removed by centrifuging the particle solution, removing the supernatant, and replacing the supernatant with purified and deionized water (two washes). Samples were dried under vacuum at room temperature. For stabilized particles, the same procedure was used, except that the initial solution of 1 g/l iron included the desired amount of stabilizer (CMC). CMC was tested at ratios of 0.0001 to 0.001 mole CMC:mole Fe.

2.3. Characterization techniques

Thermogravimetric analysis (TGA) was performed on a TGA Q5000 (TA Instruments, New Castle, DE). Samples were washed, deposited on silicon wafers, dried, and measured in ceramic sample pans. Each sample was heated from 40°C to 800°C at a rate of 10°C/min. The balance purge flow was 10 ml/min N_2, and the sample purge flow was 25 ml/min air.

Particle size and zeta potential measurements and titrations were performed on a Zetasizer Nano ZS (Malvern Instruments, Westborough, MA) using noninvasive backscatter (NIBS) detection at 173°. This instrument uses Mie theory to correlate particle size from the intensity of the light scattered from the particles; the use of Mie theory rather than the Fraunhofer approximation allows more accurate measurement of particle size in the nanometer range. At least 10 separate measurements were taken on each sample for both particle size and zeta potential; particle size and zeta potential measurements were taken as point measurements directly following particle synthesis without washing or pH adjustment, and results were repeatable from sample to sample except where noted. The pH was measured following each synthesis, and all solutions had pH values between 8.5 and 9.0. All titrations were performed starting at pH 2 and increasing to pH 12 with 0.1×10^{-3} mol/m^3 and 0.025×10^{-3} mol/m^3 NaOH. Samples were measured directly following synthesis without the washing or drying procedures mentioned above. Samples were diluted 1:20 with water and filtered with a 0.2 μm polyethersulfone syringe filter before measurement.

Particles were also characterized with field emission scanning electron microscopy (FESEM) and transmission electron microscopy (TEM). For both FESEM and

[2]Commercial equipment, instrument, or materials are identified only in order to adequately specify certain procedures. In no case does such identification imply recommendation or endorsement by the National Institute of Standards and Technology, nor does it imply that the products identified are necessarily the best available for the purpose.

TEM images, samples were centrifuged and washed with purified water to remove excess salt and were dropcast on either copper grids (TEM) or silicon wafers (FESEM). Particle composition was analyzed by energy dispersive x-ray (EDX) analysis.

3. Results and discussion

Unstabilized nanoparticle samples made from each of the two iron salts, $FeSO_4*7H_2O$ or $FeCl_3$, were observed with both FESEM and TEM. Results are shown in Fig. 1. Syntheses with both of the iron salts resulted in a mix of spherical nano-sized particles and elongated crystal structures, and no major differences in particle or crystal morphology were observed between the two syntheses. Two distinct particle size populations were visible (Fig. 1b), and the larger spherical nanoparticles formed chains (Figs. 1a and b). The larger nanoparticles were approximately 100 nm in diameter, while the smaller particles were 5 nm to 10 nm in diameter (Fig. 1d). Some lattice fringes were visible in TEM images, and diffraction patterns were obtained from the small particles, indicating that the particles are likely to be crystalline. In high-resolution TEM images, the elongated crystals had a core-shell structure with visible lattice fringes (Fig. 1c). EDX analysis of both the crystals and the nanoparticles indicated that the crystals contained more than twice the mass of oxygen (by weight %) than the spherical particles. The EDX data also confirmed that the particles and crystals were composed primarily of iron, with little to no residual sodium, chloride, or sulfate. While the larger nanoparticles were observed to form particle chains for both iron salts (results for the larger nanoparticle population from a $FeCl_3$ synthesis not shown), the smaller size population (at 5 nm to 10 nm) did not form visible chains, but rather formed irregular aggregates. This result can be seen for both iron salts in Figs. 1e and f.

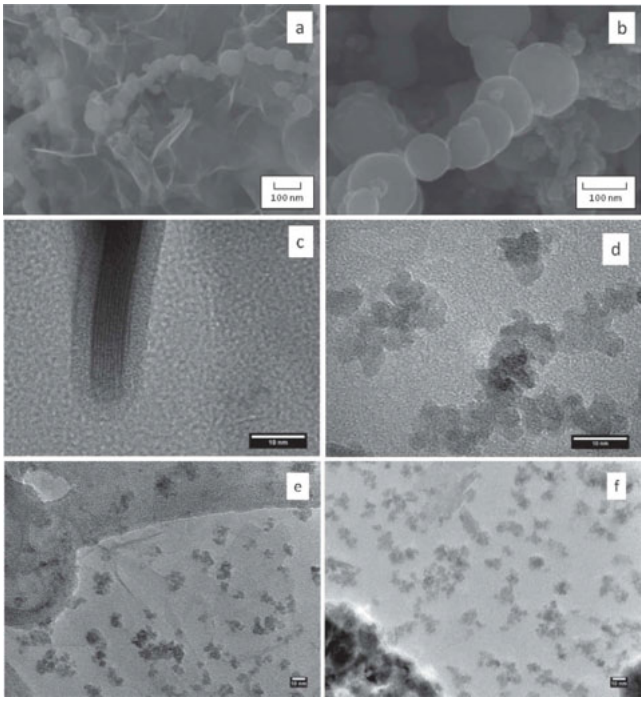

Fig. 1. FESEM and TEM images of ZVI nanoparticles synthesized without CMC stabilizer. Nanoparticles were made with (a & b) $FeSO_4*7H_2O$ (FESEM images) or (c & d) anhydrous $FeCl_3$ (TEM images). Lower resolution TEM images show characteristic aggregation of unstabilized nanoparticles for both iron starting materials (e) $FeSO_4*7H_2O$ and (f) $FeCl_3$. For both starting materials, spherical particles of two size populations and elongated crystals formed. Elongated crystals and small spherical particles displayed lattice fringes in TEM imaging. TEM scale bars are all 10 nm (c–f).

Washed samples stabilized by CMC are shown in Fig. 2 for both iron salts. The particles from each sample were spherical, with some polymer visible surrounding and in between the dispersed particles. Elongated crystals were also present after particle synthesis. The particles synthesized from $FeSO_4*7H_2O$ (Fig. 2a) were quite uniform in size and shape and appeared to be separate and stabilized. However, the particles synthesized from $FeCl_3$ (Fig. 2b), once washed, aggregated and formed chains, similar to those observed in Figs. 1a and b for the unstabilized particles. When SEM images were obtained for unwashed samples (images not shown), much more polymer was visible around the particles, but in this case, $FeSO_4*7H_2O$-synthesized particles also appeared to be stabilized while $FeCl_3$-stabilized particles appeared to form globular agglomerates with the polymer. Washing the particles appears to remove excess polymer in both samples, but the stabilization effect of CMC on the iron nanoparticles is limited for those synthesized from $FeCl_3$.

Before synthesis, when the iron salt was added to the CMC aqueous solution, the ferrous salt formed a clear, dissolved solution, while the ferric salt formed a colloidal, yellow precipitate. When sodium borohydride was added to reduce the iron and precipitate particles,

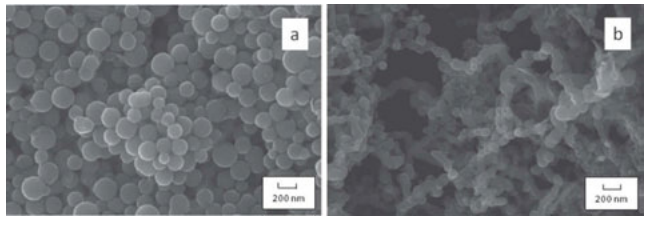

Fig. 2. FESEM images of ZVI nanoparticles and associated CMC (0.7 degree of substitution, 0.0005 mole CMC:mole Fe) polymer for (a) $FeSO_4*7H_2O$ or (b) anhydrous $FeCl_3$ as starting materials. Both iron salt starting materials resulted in similar observed particle size populations, but the ferrous salt allowed the formation of a more well-dispersed sample, with little particle aggregation, as compared to the ferric salt.

the ferrous salt solution formed a black, well-dispersed solution, with no individual particles or aggregates visible. This solution had minimal observable settling of the particle suspension over several weeks. In contrast, the ferric salt solution, when precipitated, formed a black, globular, colloidal suspension that settled within several hours.

Thermogravimetric analysis was used to determine whether stabilizer remained coordinated with the nanoparticles after washing and centrifuging, as well as to evaluate the effect of the stabilizer on the oxidation profile of the nanoparticles. Results are shown in Fig. 3. A representative oxidation profile for CMC is shown in Fig. 3a for a 0.9 degree of substitution. All three CMC stabilizers tested resulted in similar but unique profiles. All three compounds had three successive decreases in sample weight as temperature increased. The maximum weight change of the first slope was similar for the three CMC compounds at 283.2°C ± 2.7°C, with a secondary maximum at 262.2°C ± 5.2°C. For 0.7 degree and 0.9 degree of substitution, the second mass loss included two nondistinct maxima at average temperatures of 365.5°C ± 1.5°C and 406.6°C ± 2.7°C, and the third mass loss included two to three maxima between 480°C and 530°C. The CMC with a 1.2 degree of substitution had a second loss of mass with a maximum weight change at approximately 380°C and a third mass loss with several maxima between 560°C and 630°C. The specific maxima obtained in the third region of mass loss varied from sample to sample but the temperature range remained constant. The weight losses of the CMC stabilizers were 80.3% ± 3.7%, 74.7% ± 1.4%, and 68.8% ± 1.2% for 0.7, 0.9, and 1.2 degrees of substitution, respectively.

The oxidation of unstabilized iron nanoparticles (from $FeSO_4*7H_2O$) is clearly visible in the weight change profile (Fig. 3b); the oxidation starts at 450°C and ends at 585°C, with the maximum weight change occurring at approximately 500°C. There is a secondary maximum at 545°C. Nanoparticles made from $FeCl_3$ resulted in a similar profile, with the primary maximum at 470°C and the secondary maximum at 540°C. An average weight increase of approximately 33.2% ± 2.0% was observed for the unstabilized nanoparticle samples.

The presence of CMC in the nanoparticle samples resulted in a decrease in the temperatures of the maximum weight changes for both iron salts, and the secondary maximum occurred at a lower temperature before the primary maximum. Nanoparticle oxidation at lower temperatures may result from the protective coating that CMC provides on the surface of the nanoparticles. Unstabilized nanoparticle samples are more likely to have a native oxide shell on the surface of the particles that would protect the iron core from oxidation, whereas stabilized nanoparticles may not form such a shell (or as thick of a shell) due to the CMC surface coverage. Therefore, as the temperature increases during TGA, the CMC is easily removed and exposes an iron metal surface amenable to oxidation. When the two iron salts are compared, the CMC appeared to have a minimal effect on the weight change profile and overall percent weight change of the ferric salt sample, as compared to the ferrous salt sample. The decrease in the oxidation temperature in the ferric salt nanoparticles was much smaller than that observed for the ferrous salt nanoparticles, and the weight change of the ferric salt nanoparticles (32.0% ± 0.6%) was similar to that obtained for the unstabilized nanoparticles (33.2% ± 2.0%). In contrast,

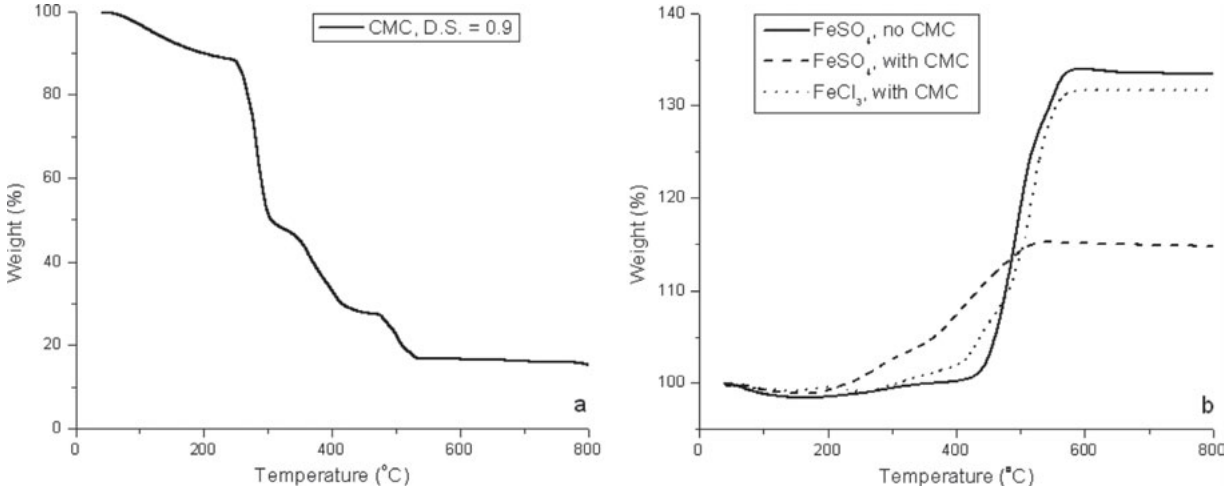

Fig. 3. TGA as change in sample weight (%) for (a) CMC polymer with a 0.9 degree of substitution and for (b) unstabilized ZVI nanoparticles from $FeSO_4*7H_2O$, CMC stabilized ZVI nanoparticles synthesized from $FeSO_4*7H_2O$, and CMC stabilized ZVI nanoparticles synthesized from $FeCl_3$. All nanoparticle samples were centrifuged and washed. CMC appears to coordinate more strongly with particles made from $FeSO_4*7H_2O$, causing greater shifts in oxidation temperatures and mass change.

the stabilized ferrous salt nanoparticles had a weight change of only 16.2% ± 2.7%, and the oxidation started at 200°C and ended at 550°C, with the primary maximum weight change occurring at 406°C. Weight change averages were obtained from at least four separate samples for each sample type.

The smaller increase in sample mass for the $FeSO_4$*$7H_2O$-synthesized particles indicates that there was stabilizer still coordinated with the ferrous salt nanoparticles, and the loss of the stabilizer through oxidation partially negated the increase in mass due to iron oxidation. This effect on weight change was not observed for the ferric salt nanoparticles, suggesting that little to no stabilizer was still coordinated with these nanoparticles after washing. Although it is possible that the smaller increase in mass for the $FeSO_4$*$7H_2O$-synthesized particles could be due to partial oxidation of the sample before TGA, the result presented in Fig. 3 was repeatedly obtained for several separate samples, and it is more likely that the presence of CMC would protect the nanoparticles from oxidation. For the $FeSO_4$*$7H_2O$ sample, the difference in mass increase represented by the stabilizer (approximately 16 wt.% of the sample, or 0.6 g) represents approximately 10% of the original mass of stabilizer added to the synthesis solution. Therefore, it appears that most of the CMC is removed when the particles are washed, and a large excess of CMC is necessary to produce the small nanoparticles observed. Lower ratios of CMC:Fe were not as effective at controlling particle size, even though there was still an excess of CMC, based on TGA results. The differences in TGA observed for $FeSO_4$*$7H_2O$-synthesized particles versus $FeCl_3$-synthesized particles further support the SEM images in Fig. 2, where $FeCl_3$-synthesized particles are aggregated and unstabilized.

Particle size distributions were obtained through dynamic light scattering (DLS). A comparison of distributions for the two iron salts with and without CMC stabilizer is shown in Fig. 4 for light scattering intensity and particle volume. Note that the modal particle diameters obtained in the volume distributions are typically 10% to 15% lower than those obtained from the intensity distributions, due to the deconvolution algorithm used by the instrument to convert scattering intensity into an intensity distribution as a function of particle size.

The unstabilized nanoparticle solutions resulted in bimodal particle size distributions with one modal particle diameter around 100 nm and one between 800 nm and 2,000 nm. These particle size distributions are similar for both the intensity and volume distributions, and no peaks are observed at particle diameters less than 50 nm. These results are in contrast to the small particles observed in FESEM and TEM images (Fig. 1), and indicate that the unstabilized samples quickly aggregated after particle synthesis, so that the smaller particles were not detectable by DLS.

When CMC was added to stabilize the nanoparticles, the smaller nanoparticles were detectable by dynamic light scattering. TEM images (data not shown) confirmed the presence of nanoparticles less than 10 nm in diameter. The two iron salts produced multimodal particle size distributions for both light scattering intensity and

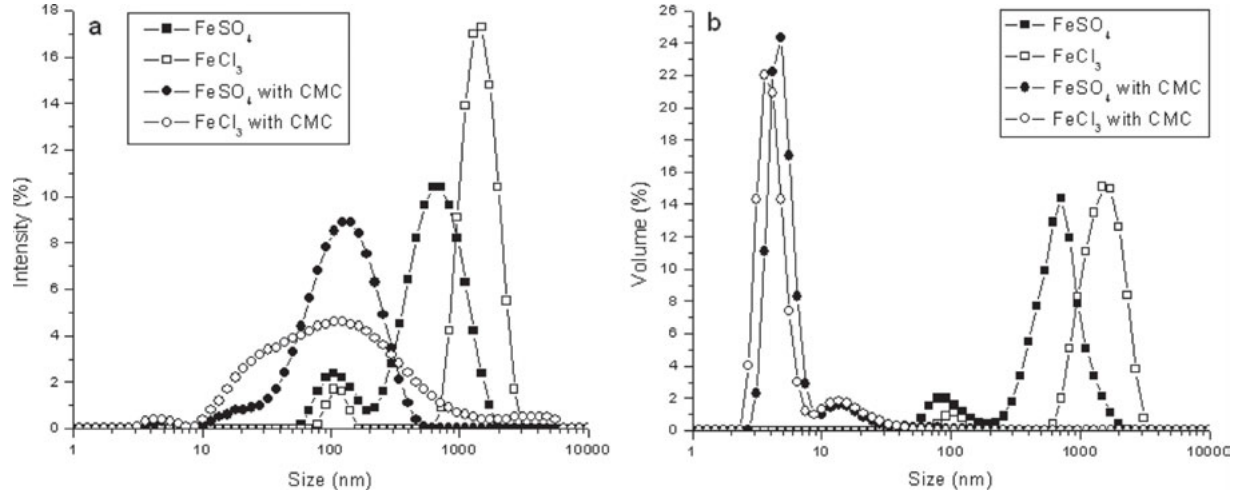

Fig. 4. Particle size distributions from dynamic light scattering obtained for (a) light scattering intensity and (b) particle volume for nanoparticles synthesized from $FeSO_4$*$7H_2O$ or $FeCl_3$, with or without CMC stabilizer. Square symbols represent unstabilized particle samples and circles represent CMC-stabilized particle samples. Stabilized samples contained CMC at a molar ratio of 0.0005 CMC:Fe and a 0.7 degree of substitution. The addition of CMC decreased the modal particle diameters for both size populations, and results are similar, but not identical, for the two iron salts.

particle volume distribution. The intensity curves typically resolved a small particle diameter of less than 10 nm, together with one to two modes between 10 and 500 nm. The modal particle diameter was typically between 100 nm and 200 nm, a result that was confirmed by the particles observed in FESEM images (Fig. 2). The volume distributions (Fig. 4b) for the stabilized particles differed significantly from the intensity distributions. The majority of the particle volume of the stabilized samples was in the particle population with a modal diameter of less than 10 nm, with a small portion of the particle volume representing particles greater than 10 nm. Furthermore, the intensity distribution for the ferric salt nanoparticles typically had broad, unresolved peaks, while the ferrous salt particles had more well defined modal diameters. This difference in the particle size distributions disappeared in the volume distribution, and the two stabilized nanoparticle sample volume distributions were quite similar. This wide distribution in $FeCl_3$ nanoparticle size around the second modal diameter was not observed in FESEM images, and is likely a result of excess colloidal CMC measured by DLS as part of the sample. DLS measurements of CMC alone resulted in unimodal diameters above 1000 nm.

Several different molar ratios of CMC:Fe were tested with $FeSO_4*7H_2O$ in nanoparticle synthesis. A comparison of particle size distributions is shown in Fig. 5a. All molar ratios resulted in bimodal particle size distributions, but the largest ratio of 0.001 resulted in a much smaller second mode. The molar ratio of 0.0005 resulted in the smallest modal particle diameter (5.3 nm ± 2.5 nm), and the molar ratio of 0.001 resulted in a statistically insignificant increase in the smallest mode. The two lower molar ratios of 0.0001 and 0.00025 resulted in an increase in the two modal particle diameters, with the smaller modes at 17.0 nm ± 2.0 nm and 12.0 nm ± 4.3 nm, respectively. These results indicate that, for the ratios tested, a ratio of 0.0005 was the optimal choice to produce nanoparticles with a diameter of less than 10 nm; smaller ratios allowed larger particles to form, and the larger ratio of 0.001 did not decrease the modal particle diameter further. Future degradation studies with representative water contaminants will indicate if these differences in particle size and CMC:Fe ratio affect particle reactivity.

The effect of the degree of carboxyl functional group substitution on nanoparticle size was tested, and a comparison for the three CMC compounds is shown in Fig. 5b. The lowest degree of substitution resulted in the smallest modal particle diameter (3.4 nm ± 2.1 nm), with 0.9 degree of substitution having a modal particle diameter of 7.0 nm ± 1.2 nm and 1.2 degree of substitution having a modal diameter of 4.5 nm ± 2.8 nm. All three types of CMC resulted in bimodal distributions; however the CMC with the lowest degree of substitution had a smaller fraction of the particle volume in the second mode. This CMC appears to be the best choice in producing the smallest nanoparticles within the conditions tested in this study.

The different molar ratios of CMC:Fe and the different types of CMC did not result in differences in sample zeta potential. However, there were differences observed for the two iron salts and between stabilized and unstabilized nanoparticles. The zeta potential measurements of stabilized and unstabilized nanoparticle samples

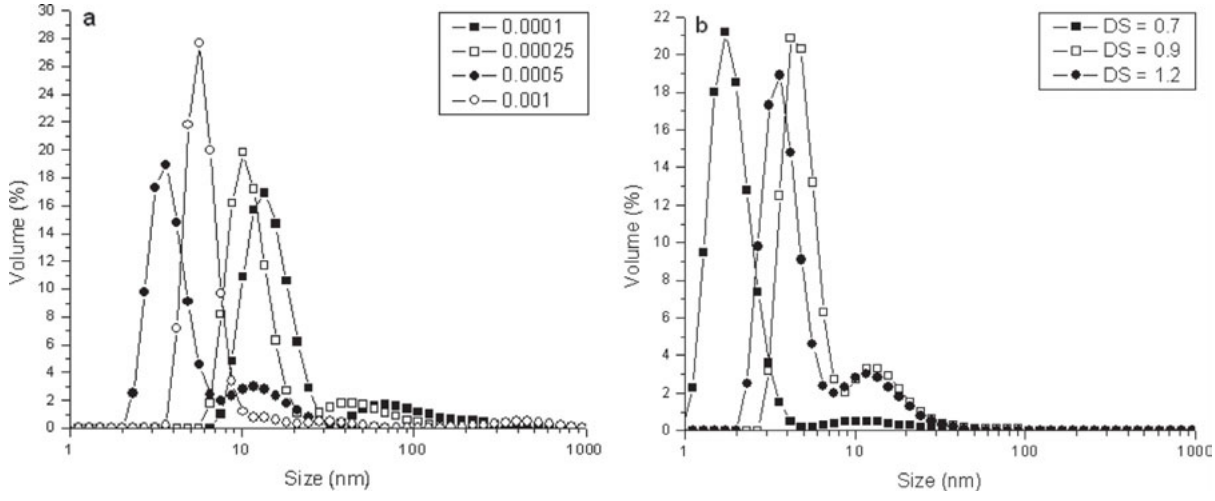

Fig. 5. Particle size distributions from dynamic light scattering for $FeSO_4*7H_2O$ nanoparticle samples with (a) four molar ratios of CMC:Fe (0.0001–0.001) and (b) CMC with three different degrees of substitution (DS). All samples in (a) contained CMC with a 1.2 degree of substitution. All samples in (b) contained a CMC molar ratio of 0.0005. Results are shown as particle volume %, and differences in modal particle diameter illustrate the effect of CMC concentration and degree of carboxyl substitution on particle size.

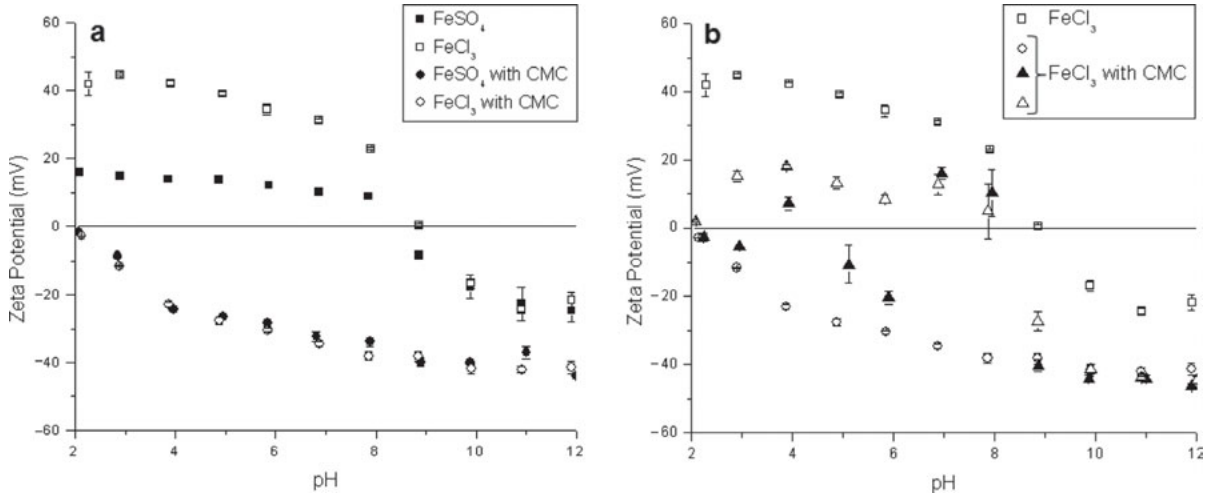

Fig. 6. Measurements of zeta potential for nanoparticle samples made with either $FeSO_4$*$7H_2O$ or $FeCl_3$, with and without CMC stabilizer. In part (a), zeta potential as a function of pH is compared for both starting materials with and without CMC stabilizer. In part (b), the variability of zeta potential measurements is displayed for CMC-stabilized particles made from $FeCl_3$. Samples represented by open and closed triangles were mixed for 10 min to 20 min before $NaBH_4$ addition, while open circles represent a sample that was mixed for 30 min before $NaBH_4$ addition. This variability is not observed for samples made from $FeSO_4$*$7H_2O$. Error bars are displayed for all data points.

synthesized from the two iron salts are compared in Fig. 6 as a function of pH. The unstabilized sample synthesized from $FeCl_3$ had a much higher zeta potential at pH values below pH 9, but the samples had similar isoelectric points (IEPs) around pH 9 and quite similar zeta potential values at pH values above the IEP. In contrast, the stabilized nanoparticle samples shown in Fig. 6a had negative zeta potentials throughout the entire pH range tested; this shift in zeta potential was likely due to the presence of CMC. The carboxyl groups of the stabilizer have pKa values less than 4.0, which indicates that most of the carboxyl groups were deprotonated over most of the pH range tested [18]. Below a pH of 4.0, it is likely that some of the carboxyl groups became protonated, which resulted in the approach of the zeta potential towards zero at pH 2 to 3. The results in Fig. 6a suggest that the zeta potential trend for the stabilized nanoparticles was similar even though the particles were synthesized from different starting iron salts. However, although the data were easy to repeat for particles synthesized from $FeSO_4$*$7H_2O$, several samples synthesized from $FeCl_3$ produced drastically different results, as shown in Fig. 6b. The data for $FeCl_3$ particles that were most similar to the $FeSO_4$*$7H_2O$ data resulted from a sample that was mixed for a longer period (30 min) before the addition of sodium borohydride. Shorter mixing periods of 10 min to 20 min resulted in zeta potential trends denoted by the open and closed triangles in Fig. 6b. The variability in zeta potential, along with the results presented above for TGA and the colloidal precipitate observed in solution, strongly suggest that the nanoparticles synthesized from $FeCl_3$ do not coordinate well with CMC and do not form a stable and well-dispersed aqueous solution.

4. Conclusions

Based on the results of this study, the CMC stabilizer produced stable, well-dispersed ZVI nanoparticle solutions when particles are synthesized from $FeSO_4$*$7H_2O$; $FeCl_3$-synthesized particles form unstable, colloidal precipitates. Electron microscopy confirmed the presence of two particle size populations in both stabilized and unstabilized nanoparticle samples, as well as the presence of elongated iron crystals; however, the stabilizer kept particles dispersed, while the unstabilized samples quickly aggregated and formed chains of particles, with no smaller particles (<50 nm) detectable by dynamic light scattering. TGA revealed that little to no CMC remained coordinated with ZVI nanoparticles synthesized from $FeCl_3$ after the sample was washed. Particle size distributions were largely bimodal, and the addition of CMC decreased the modal particle diameter of both modes. The smallest modal diameter was obtained for CMC-stabilized particles at a CMC:Fe molar ratio of 0.0005 and 0.7 degree of substitution.

Acknowledgements

The authors acknowledge Roy H. Geiss for his work obtaining the TEM images, as well as Ann N. Chiaramonti, Robert R. Keller, and Nicholas Barbosa III for their help with FESEM imaging and EDX analysis.

References

[1] Z.X. Tang, C.M. Sorensen, K.J. Klabunde and G.C. Hadjipanayis, Size-Dependent curie temperature in nanoscale $MnFe_2O_4$ particles, Phys. Rev. Lett., 67(25) (1991) 3602–3605.

[2] S. Chattopadhyay, P. Ayyub, V.R. Palkar and M. Multani, Size-induced diffuse phase transition in the nanocrystalline ferroelectric $PbTiO_3$, Phys. Rev. B., 52(18) (1995) 13177–13183.

[3] M. Auffan, J. Rose, J.Y. Bottero, G.V. Lowry, J.P. Jolivet and M.R. Wiesner, Towards a definition of inorganic nanoparticles from an environmental, health and safety perspective, Nat. Nanotechnol., 4(10) (2009) 634–641. 10.1038/nnano.2009.242.

[4] A.J. Feitz, S.H. Joo, J. Guan, Q. Sun, D.L. Sedlak and T.D. Waite, Oxidative transformation of contaminants using colloidal zero-valent iron, Colloids Surf. A., 265(1–3) (2005) 88–94.

[5] C.R. Keenan and D.L. Sedlak, Factors affecting the yield of oxidants from the reaction of manoparticulate zero-valent iron and oxygen, Environ. Sci. Technol., 42(4) (2008) 1262–1267.

[6] B. Schrick, J.L. Blough, A.D. Jones and T.E. Mallouk, Hydrodechlorination of trichloroethylene to hydrocarbons using bimetallic nickel-iron nanoparticles, Chem. Mater., 14(12) (2002) 5140–5147. 10.1021/cm020737i.

[7] S.M. Ponder, J.G. Darab, J. Bucher, D. Caulder, I. Craig, L. Davis, N. Edelstein, W. Lukens, H. Nitsche, , L.F. Rao, D.K. Shuh and T.E. Mallouk, Surface chemistry and electrochemistry of supported zerovalent iron nanoparticles in the remediation of aqueous metal contaminants, Chem. Mater., 13(2) (2001), 479–486. 10.1021/cm000288r.

[8] Y.H. Kim and E.R. Carraway, Dechlorination of chlorinated ethenes and acetylenes by palladized iron, Environ. Technol., 24(7) (2003) 809–819.

[9] G.K. Parshetti and R.A. Doong, Immobilization of bimetallic nanoparticles on microfiltration membranes for trichloroethylene dechlorination, Water Sci. Technol., 58(8) (2008) 1629–1636.

[10] Y.C. Lee, C.W. Kim, J.Y. Lee, H.J. Shin and J.W. Yang, Characterization of nanoscale zero valent iron modified by nonionic surfactant for trichloroethylene removal in the presence of humic acid: A research note, Desalin. Water Treat., 10(1–3) (2009) 33–38.

[11] F. He, D.Y. Zhao, J.C. Liu and C.B. Roberts, Stabilization of Fe-Pd nanoparticles with sodium carboxymethyl cellulose for enhanced transport and dechlorination of trichloroethylene in soil and groundwater, Ind. Eng. Chem. Res., 46(1) 2007) 29–34. 10.1021/ie0610896.

[12] Z.H. Zheng, S.H. Yuan, Y. Liu, X.H. Lu, J.Z. Wan, X.H. Wu and J. Chen, Reductive dechlorination of hexachlorobenzene by Cu/Fe bimetal in the presence of nonionic surfactant, J. Hazard. Mater., 170(2–3) (2009) 895–901. 10.1016/j.jhazmat.2009.05.052.

[13] F. He and D.Y. Zhao, Preparation and characterization of a new class of starch-stabilized bimetallic nanoparticles for degradation of chlorinated hydrocarbons in water, Environ. Sci. Technol., 39(9) (2005) 3314–3320. 10.1021/es048743y.

[14] F. He and D.Y. Zhao, Manipulating the size and dispersibility of zerovalent iron nanoparticles by use of carboxymethyl cellulose stabilizers, Environ. Sci. Technol., 41(17) (2007) 6216–6221. 10.1021/es0705543.

[15] R.A. Doong and Y.J. Lai, Dechlorination of tetrachloroethylene by palladized iron in the presence of humic acid, Water Res., 39(11) (2005) 2309–2318. 10.1016/j.watres.2005.04.036.

[16] F. He and D.Y. Zhao, Hydrodechlorination of trichloroethylene using stabilized Fe-Pd nanoparticles: Reaction mechanism and effects of stabilizers, catalysts and reaction conditions, Appl. Catal., B., 84 (2008) 533–540.

[17] Y.H. Lin, H.H. Tseng, M.Y. Wey and M.D. Lin, Characteristics, morphology and stabilization mechanism of PAA250K-stabilized bimetal nanoparticles, Colloids Surf. A., 349(1–3) (2009) 137–144. 10.1016/j.colsurfa.2009.08.007.

[18] T. Heinze and A. Koschella, Carboxymethyl ethers of cellulose and starch - A review, Macromol. Symp., 223 (2005) 13–39. 10.1002/masy.200550502.